

Sitting at the edge: How biomolecules use hydrophobicity to tune their interactions and function

Amish J. Patel¹, Patrick Varilly², Sumanth N. Jamadagni¹,
Michael F. Hagan³, David Chandler^{2,*}, & Shekhar Garde^{1,*}

¹Howard P. Isermann Department of Chemical & Biological Engineering,
and Center for Biotechnology & Interdisciplinary Studies,
Rensselaer Polytechnic Institute, Troy, NY, 12180, USA.

²Department of Chemistry, University of California, Berkeley, CA, 94720, USA.

³Martin A. Fisher School of Physics, Brandeis University, Waltham, MA 02454, USA.

*To whom correspondence should be addressed: gardes@rpi.edu, chandler@berkeley.edu

Abstract

Water near hydrophobic surfaces is like that at a liquid-vapor interface, where fluctuations in water density are substantially enhanced compared to that in bulk water. Here we use molecular simulations with specialized sampling techniques to show that water density fluctuations are similarly enhanced, even near hydrophobic surfaces of complex biomolecules, situating them at the edge of a dewetting transition. Consequently, water near these surfaces is sensitive to subtle changes in surface conformation, topology, and chemistry, any of which can tip the balance towards or away from the wet state, and thus significantly alter biomolecular interactions and function. Our work also resolves the long-standing puzzle of why some biological surfaces dewet and other seemingly similar surfaces do not.

Much of biology happens in aqueous environments, with interfaces of biomolecules being wet [1,2]. Yet, hydrophobically driven assembly leads to contact surfaces that contain little or no water [3,4]. How biomolecules are able to perform the task of removing water from their vicinity is an important open question [5]. Here, we show that the answer lies in the proximity of water near hydrophobic surfaces to an underlying phase transition. Thermodynamically, water at ambient conditions is already close to the liquid-vapor phase boundary. Near a hydrophobic surface, water molecules are pulled away from the surface, because they interact only weakly with the surface, but have strong hydrogen bonding interactions with water in the bulk. This further destabilizes water near hydrophobic surfaces and pushes it close to the edge of a dewetting transition. Indeed, idealized repulsive hydrophobic surfaces nucleate a soft liquid-vapor like interface [6–8]. However, weak attractive van der Waals forces exerted by realistic hydrophobic surfaces pull the soft interface closer, rewetting the surface, and

masking the proximity to the underlying dewetting transition [9–12]. This proximity is then revealed not by the mean water density near the surface, but instead by fluctuations away from the mean [13], and by the response of water density to perturbations [8, 9].

Here we employ specialized sampling techniques [13, 14] to measure water density fluctuations near complex biomolecular surfaces, and show that they can be enhanced near a sufficiently hydrophobic patch. Further, we demonstrate the sensitivity of water density to perturbations near such surfaces. It is by exploiting this sensitivity to perturbations, *e.g.*, through subtle conformational changes, that biomolecules are able to dewet their surfaces. This near-the-edge behavior can also be important in the function of certain biomolecules, such as in the vapor-lock gating of ion channels. Our results also explain why the gap between two hydrophobic protein surfaces was found to be wet in one case [2], and dry in another [15]: the two systems are close to, but on either side of the dewetting transition.

To illustrate that water density fluctuations provide a clear signature of hydrophobicity, we characterize them near self-assembled monolayer (SAM) surfaces with $-\text{CH}_3$ and $-\text{OH}$ head groups, and in bulk water (Fig. 1A). Specifically, we calculate the probability distribution, $P_v(N)$, of observing N water molecules in a volume, v , of interest (see Supplementary Information below). The average number, $\langle N \rangle$, of water molecules in v , reflected in the peak of $P_v(N)$, is similar in all three cases, indicating that both the $-\text{CH}_3$ and the $-\text{OH}$ SAMs are wet. The density fluctuations in bulk water and at the hydrophilic $-\text{OH}$ SAM are also similar and approximately Gaussian (parabolic on a log scale), as expected [13]. However, fluctuations near the hydrophobic $-\text{CH}_3$ SAM are different, with $P_v(N)$ enhanced significantly for low N -values [13]. Because the differences in the distributions at low N correspond to fluctuations that are extremely rare, *i.e.*, $P_v(N)$ is very small, they do not affect the average equilibrium behavior. However, these rare fluctuations play an important role in the presence of a perturbation. For example, the response of water near the $-\text{CH}_3$ and $-\text{OH}$ surfaces to an unfavorable linear potential, ϕN , is very different. Near the $-\text{OH}$ surface, increasing ϕ shifts the distribution to the left (Fig. 1C), and lowers the mean density of water, $\langle N \rangle_\phi$, gradually (Fig. 1E). In contrast, near the $-\text{CH}_3$ surface, even small ϕ -values, of the order of the thermal energy ($k_B T$), are sufficient to dramatically alter the distribution, with low- N fluctuations being enhanced so much that they become the most probable ones (Fig. 1D). As a result, even a small perturbation is able to dry the hydrophobic $-\text{CH}_3$ surface, and $\langle N \rangle_\phi$ decreases precipitously (Fig. 1E). Correspondingly, the sensitivity of water density to perturbations, quantified by the susceptibility, $\partial \langle N \rangle_\phi / \partial \phi$, displays a peak near the hydrophobic surface (Fig. 1F); a known feature of phase transitions. Thus, the remarkable sensitivity of water density to perturbations is directly connected to the enhanced low- N fluctuations, with both observations resulting from the proximity of water to an underlying dewetting transition [7–9, 13].

To explore whether the principles governing the dewetting of hydrophobic interfaces illustrated above extend to the topologically and chemically complex surfaces of biomolecules, we study a subunit of the enzyme BphC, which includes a large hydrophobic patch at the boundary between its two domains [2]. The protein surface is rugged (Fig. 2A), which makes the calculation of $P_v(N)$ in volumes that complement the protein surface challenging. To

this end, we developed an extension of the indirect umbrella sampling (INDUS) method [14] that enables the sampling of $P_v(N)$ in arbitrarily shaped volumes. Fig. 2B shows that $P_v(N)$ near a hydrophilic patch is bulk-like, similar to that near the -OH SAM. In contrast, despite the presence of a highly polar backbone and possible interactions with charged side chains and counter-ions, $P_v(N)$ near a hydrophobic patch on the isolated domain I surface shows enhanced low- N fluctuations (Fig. 2C), similar to that demonstrated for the -CH₃ SAM.

To investigate how water near the hydrophobic patch responds to realistic perturbations, we place domain II near domain I at different separations, Δz , and calculate $P_v(N)$ in the space between the two domains. As the domains are brought closer, while the likelihood of drying [$P_v(N \approx 0)$] increases (Fig. 2D), the inter-domain region remains wet. Even at $\Delta z = 0.4$ nm, where only a single layer of water can be accommodated between the domains, the average value of N [peak of $P_v(N)$] is high, consistent with the findings of Ref. [2]. This might seem surprising given the prevalence of hydrophobic residues on the protein surfaces surrounding the inter-domain region. However, $P_v(N)$ distributions at all Δz display enhanced low- N fluctuations, suggesting that water is at the edge of a dewetting transition, albeit on the wet side. If this is indeed the case, a sufficient additional perturbation should be able to push it over the edge and trigger dewetting. To test this, and motivated by Zhou *et al.* [2], we turned off the partial charges on the protein, which is expected to be an unfavorable perturbation, and disfavor the presence of water. As a result, the hydrophobicity of the patch on the isolated domain I surface is enhanced, as reflected in the enhanced fluctuations in Fig. 2C. The effect of this perturbation on water in the inter-domain region is dramatic: an essentially dry state is now preferred even at a distance of 0.6 nm between the domain surfaces (Fig. 2E).

In contrast to the assembly of BphC domains, that of melittin dimers represents a system which sits on the dry side of the dewetting transition [15]. We calculated $P_v(N)$ near the putative hydrophobic face of an isolated dimer surface (Fig. 3A), which indeed displays enhanced fluctuations (Fig. 3B), as expected. Correspondingly, when the system is perturbed by placing a second wild-type dimer nearby, a drying transition in the space between the dimers is clearly seen in the $P_v(N)$ distributions in Fig. 3C. For $\Delta z = 0.9$ nm, the average value of N [peak of $P_v(N)$] is high, implying a wet state; whereas for $\Delta z = 0.6$ nm, the space between the dimers is dry. Interestingly, for intermediate $\Delta z = 0.7, 0.8$ nm, the $P_v(N)$ distributions show bimodal behavior, indicating the presence of a desolvation barrier separating the wet (high N) and the dry (low N) states. Barriers along this simple order parameter, N , can play an important role in governing the kinetics of dimer-dimer assembly.

Although a drying transition is observed for the wild-type melittin dimers, once again, it is extremely sensitive to small perturbations, such as point mutations, as noted by Berne and co-workers [15]. We calculated $P_v(N)$ distributions near six isolated melittin dimer mutants, which all show enhanced fluctuations, with subtle differences between them (see Fig. S1). To highlight the effect of a perturbation on the drying transition in melittin, we selected a point mutant, Ile20Gly (Fig. 3A). There are only subtle differences in the $P_v(N)$ distributions near the isolated wild-type and the mutant dimer (Fig. 3B). However, they translate into dramatic differences in confinement, where the system is poised at the edge of a dewetting

transition. Specifically, the Ile20Gly mutant no longer displays a drying transition, as the average value of N remains high even at the smallest Δz (Fig. 3D). Thus, the data in Figs. 2 and 3 underscore that both BphC and melittin sit near the edge of a wetting-dewetting transition, one on the wet and the other on the dry side, and each can be pushed to the other side by a small perturbation. This proximity to the phase transition is not evident in the mean behavior of water, but is revealed by water density fluctuations.

To enable regulation, biological systems are generically thought to position themselves near phase transitions [16]. Our application of specialized techniques that measure rare fluctuations allowed us to highlight that water near hydrophobic surfaces of biomolecules is similarly situated at the edge of a dewetting transition, and is sensitive to small perturbations. This sensitivity provides biomolecules with the powerful ability to tune their interactions and function by manipulating the local context, for example, by confining water between them, or by changing their shape or chemistry [17–19]. Given that desolvation is a component of the reaction coordinate for hydrophobically driven assembly [20], manipulating wetting-dewetting may appreciably influence the kinetics of assembly. Dewetting transitions are also central in the function of some ion channels (*e.g.*, mechano sensitive channel MscS), where a 10-20 Å long interior hydrophobic wall of the channel provides gating by the “vapor lock” mechanism – a wet channel conducts ions rapidly; whereas, a small conformational change can dry the channel and stop ion conduction completely [21–23]. Dewetting can also be induced by manipulating solution conditions (*e.g.*, temperature, pressure, pH, and co-solvent or solute concentration) [18, 24, 25]. Finally, the sensitivity of nanoscale dewetting transitions is also responsible for the spontaneous filling and emptying of hydrophobic nanotubes [26], and can be harnessed in various other non- biological settings, ranging from switches in nanofluidic devices and networks [25], to aqueous solution based catalysis in hydrophobic zeolites [27].

Acknowledgments

SG acknowledges partial financial support from NSF (CBET-0967937) and NSEC (DMR-0642573) grants. DC acknowledges financial support from NIH (R01-GM078102-04) grant. MFH acknowledges financial support from NIH (NIAID R01-AI080791) grant. We also thank Hari Acharya, Ravi Kane, and Kafui Tay for helpful discussions.

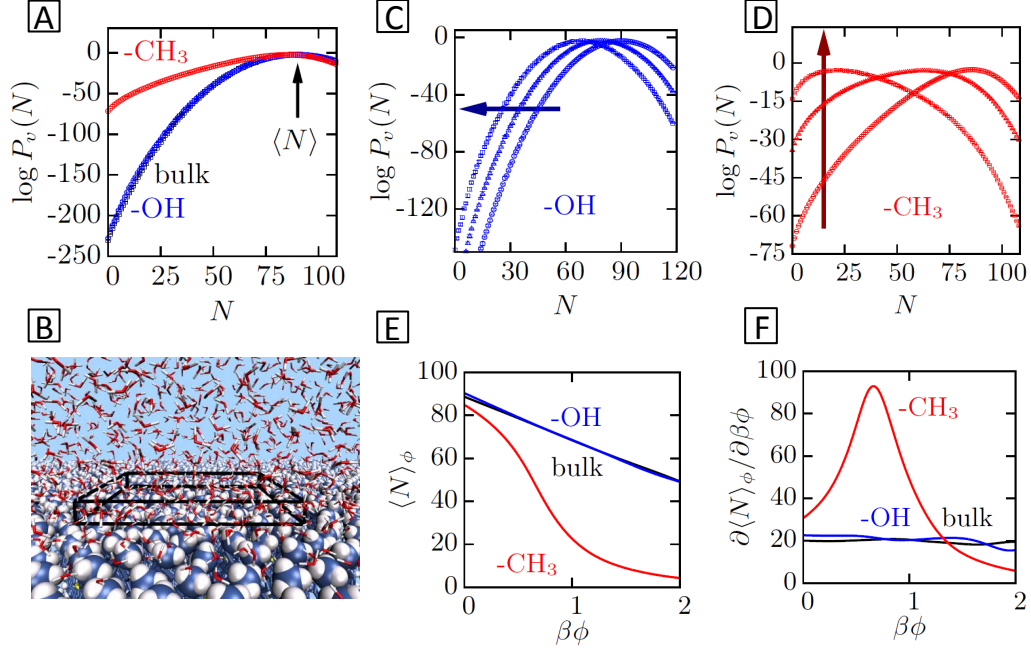


Figure 1: Water density fluctuations and its response to perturbations near hydrophobic and hydrophilic interfaces. (A) $P_v(N)$ in a $3 \text{ nm} \times 3 \text{ nm} \times 0.3 \text{ nm}$ cuboid in bulk water and at the interface of a self-assembled monolayer (SAM) with hydrophobic (-CH₃) and hydrophilic (-OH) head groups. (B) A close-up view of the hydrophobic -CH₃ SAM-water interface. Water [sticks, red (oxygen) and white (hydrogen)], -CH₃ head groups [spacefill, purple (carbon), and white (hydrogen)], and the cuboid observation volume (black wireframe) are shown. (C) and (D) $P_v(N)$ distributions near the -OH and the -CH₃ SAMs, respectively, in the presence of an unfavorable linear potential, ϕN , for $\phi = 0$ (no perturbation), and $\phi = 0.5 k_B T$ and $1 k_B T$. The arrow points in the direction of increasing ϕ . (E) The response of the average number of water molecules in the cuboid volume, $\langle N \rangle_\phi$, to the external potential ϕ , and (F) the corresponding susceptibility, $\partial \langle N \rangle_\phi / \partial \beta\phi$, show signatures of a nanoscopic phase transition near the -CH₃ surface. Error-bars calculated using six separate simulation blocks are smaller than the symbols used.

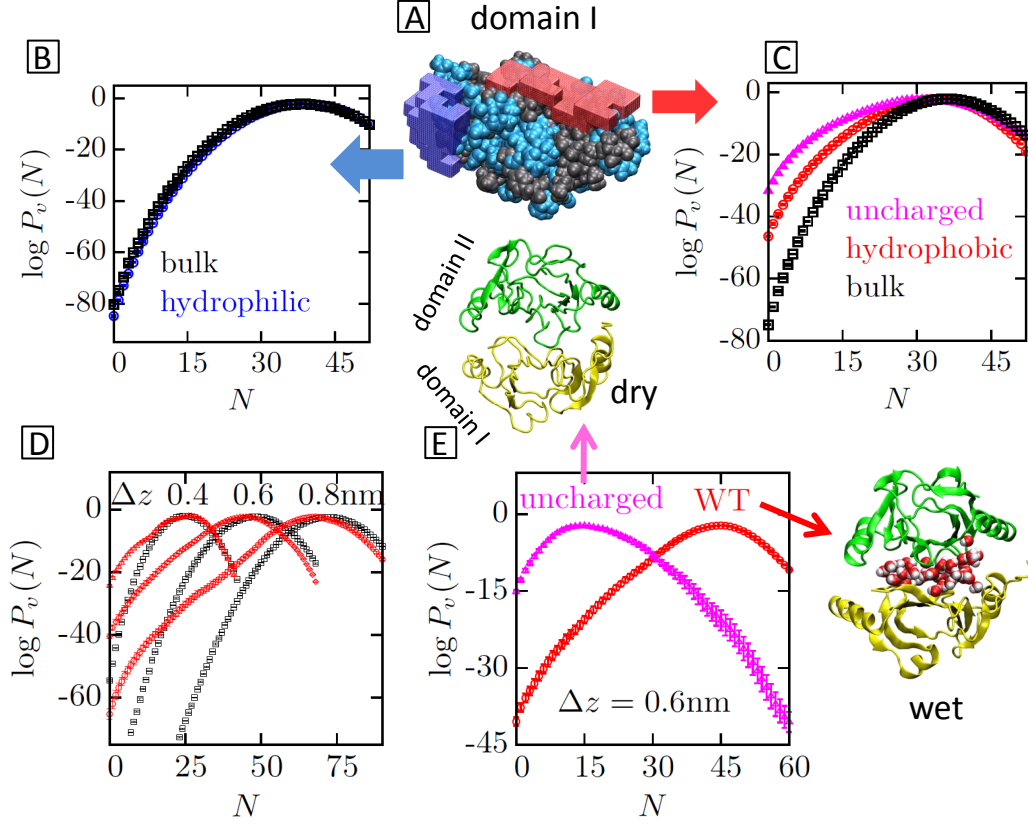


Figure 2: Density fluctuations and the corresponding wetting and drying of BphC domains. (A) A snapshot of domain I (residues 1-135) of a BphC subunit (PDB: 1DHY) showing hydrophobic (gray) and hydrophilic (blue) regions. Two separate 0.3 nm thick observation volumes complementing the protein surface near a hydrophobic (red) and a hydrophilic patch (blue), are also shown. (B) $P_v(N)$ near the hydrophilic patch is similar to that in bulk water. (C) $P_v(N)$ near the hydrophobic patch displays enhanced low- N fluctuations. When electrostatic interactions between the protein and the water are turned off, the fluctuations are enhanced further, indicating that the protein surface becomes more hydrophobic. (D) $P_v(N)$ distributions in an observation volume sandwiched between the two domains of the BphC subunit for different inter-domain separations, $\Delta z = 0.8, 0.6$, and 0.4 nm (red). Distributions in similar volumes in bulk water are shown for comparison (black). (E) $P_v(N)$ distributions in the inter-domain region for $\Delta z = 0.6$ nm, for proteins with charges on [same as in (D)] and off. Water and protein were represented using the TIP3P model and the AMBER-94 force field, respectively. Error-bars were calculated using six separate simulation blocks.

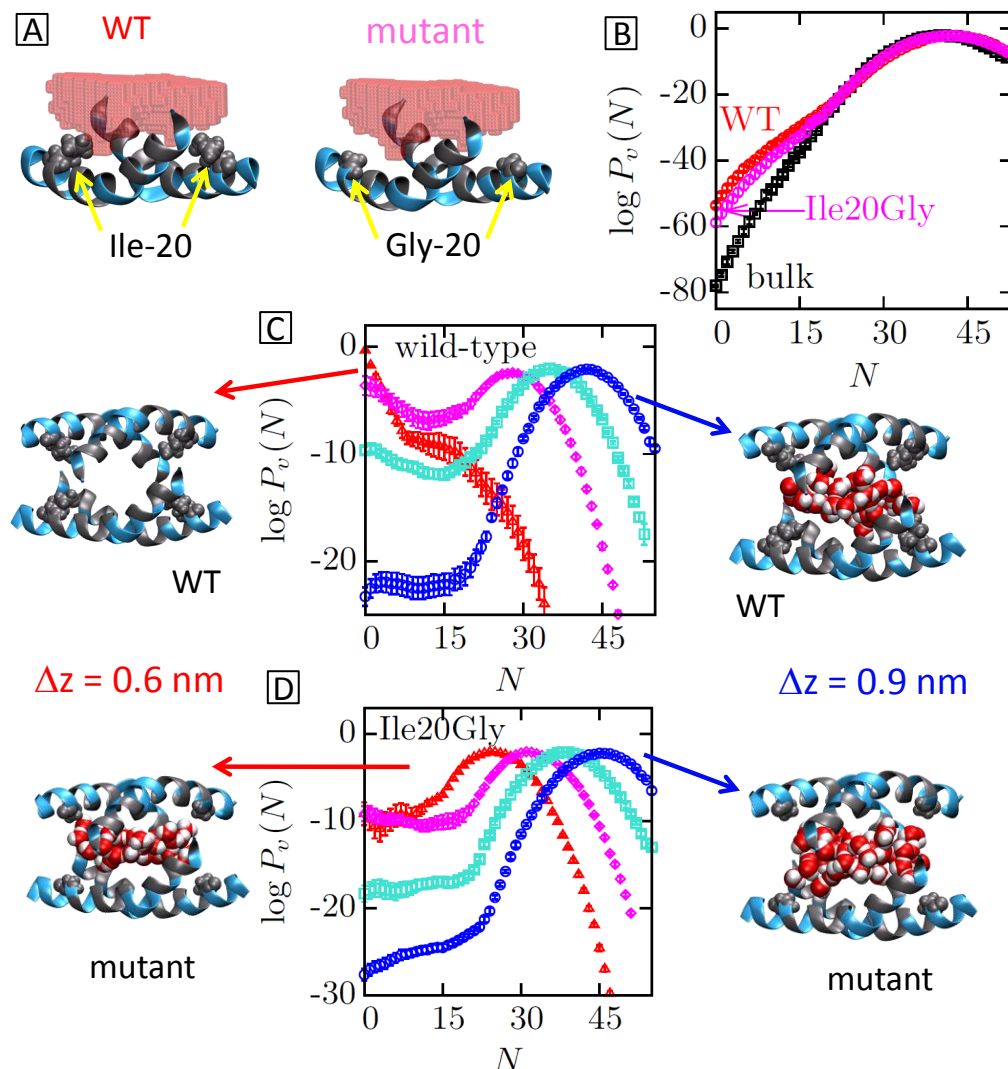


Figure 3: Melittin dimer association – sitting on the dry side. (A) A snapshot highlighting the observation volume near the hydrophobic surface of the wild type melittin dimer (PDB: 2MLT) and the Ile20Gly mutant dimer. The mutation is shown in spacefill representation. (B) $P_v(N)$ distributions in the observation volumes shown in (A) and in a similar volume in bulk water. (C) $P_v(N)$ distributions in the observation volume between two WT melittin dimers for dimer-dimer separations, Δz , of 0.9 (blue), 0.8 (cyan), 0.7 (magenta), and 0.6 nm (red), indicate a dewetting transition for $\Delta z < 0.7$ nm. Representative snapshots of the tetramer at $\Delta z = 0.6$ (dry) and 0.9 nm (wet) are shown. (D) Same as in (C) for the Ile20Gly mutants, where no dewetting is observed. Water and protein were represented using the SPC/E model and the AMBER-99sb force field, respectively. Error-bars were calculated using six separate simulation blocks.

References

- [1] Y. Cheng, P. Rossky, *Nature* **392**, 696 (1998).
- [2] R. Zhou, X. Huang, C. J. Margulis, B. J. Berne, *Science* **305**, 1605 (2004).
- [3] T. A. Larsen, A. J. Olson, D. S. Goodsell, *Structure* **6**, 421 (1998).
- [4] F. Rodier, R. P. Bahadur, P. Chakrabarti, J. Janin, *Prot. Struc. Func. Bioinform.* **60**, 36 (2005).
- [5] M. G. Krone, *et al.*, *J. Am. Chem. Soc.* **130**, 11066 (2008).
- [6] F. H. Stillinger, *J. Solution Chem.* **2**, 141 (1973).
- [7] K. Lum, D. Chandler, J. D. Weeks, *J. Phys. Chem. B* **103**, 4570 (1999).
- [8] D. Chandler, *Nature* **437**, 640 (2005).
- [9] D. M. Huang, D. Chandler, *J. Phys. Chem. B* **106**, 2047 (2002).
- [10] C.-Y. Lee, J. A. McCammon, P. J. Rossky, *J. Chem. Phys.* **80**, 4448 (1984).
- [11] R. Godawat, S. N. Jamadagni, S. Garde, *Proc. Natl. Acad. Sci. U.S.A.* **106**, 15119 (2009).
- [12] M. Mezger, *et al.*, *Proc. Natl. Acad. Sci. U.S.A.* **103**, 18401 (2006).
- [13] A. J. Patel, P. Varilly, D. Chandler, *J. Phys. Chem. B* **114**, 1632 (2010).
- [14] A. J. Patel, P. Varilly, D. Chandler, S. Garde, *J. Stat. Phys.* p. accepted (2011).
- [15] P. Liu, X. Huang, R. Zhou, B. J. Berne, *Nature* **437**, 159 (2005).
- [16] T. Mora, W. Bialek, *J. Stat. Phys.* **143**, 1 (2011).
- [17] O. Beckstein, M. S. P. Sansom, *Phys. Biol.* **1**, 42 (2004).
- [18] N. Giovambattista, C. F. Lopez, P. J. Rossky, P. G. Debenedetti, *Proc. Natl. Acad. Sci. U.S.A.* **105**, 2274 (2008).
- [19] H. Acharya, S. Vembanur, S. N. Jamadagni, S. Garde, *Faraday Discuss.* **146**, 353 (2010).
- [20] P. R. ten Wolde, D. Chandler, *Proc. Natl. Acad. Sci. U.S.A.* **99**, 6539 (2002).
- [21] A. Anishkin, S. Sukharev, *Biophys. J.* **86**, 2883 (2004).
- [22] N. Chakrabarti, C. Neale, J. Payandeh, E. F. Pai, R. Pomès, *Biophys. J.* **98**, 784 (2010).
- [23] F. Zhu, G. Hummer, *Proc. Natl. Acad. Sci. U.S.A.* **107**, 19814 (2010).

- [24] L. Hua, R. Zangi, B. J. Berne, *J. Phys. Chem. C* **113**, 5244 (2009).
- [25] J. C. Rasaiah, S. Garde, G. Hummer, *Ann. Rev. Phys. Chem.* **59**, 713 (2008).
- [26] G. Hummer, J. C. Rasaiah, J. P. Noworyta, *Nature* **414**, 188 (2001).
- [27] M. Moliner, Y. Roman-Leshkov, M. E. Davis, *Proc. Natl. Acad. Sci. U.S.A.* **107**, 6164 (2010).

Supplementary Information

Materials and Methods

All simulations were performed using the GROMACS molecular dynamics package, suitably modified to allow for importance sampling in the NVT ensemble ($T = 300$ K) with a buffering vapor-liquid interface. Here, we provide further details of the BphC and melittin simulations. We also describe how we select probe volumes to monitor water density fluctuations near proteins.

BphC: Domain I of BphC was solvated in ~ 7500 TIP3P water molecules, whereas simulations of both domains I and II contained ~ 9500 waters. To study the region between the two domains, domain II was translated along the vector joining the center of masses of the two domains by 0.4, 0.6 and 0.8 nm from the crystal structure (PDB: 1DHY). 21 atoms in each domain of BphC were position restrained harmonically. Bonds involving hydrogen atoms were constrained using the SHAKE algorithm, and temperature was maintained at 300K using the Berendsen thermostat.

To select a probe volume near a hydrophobic patch in the hydration shell of the protein (Fig. 2a), a cubic grid with a spacing of 0.3 nm was placed in the simulation box. A sufficiently large, contiguous patch of ~ 40 grid cells was then chosen as the probe volume, such that (i) no cell contained protein heavy atoms, (ii) each cell was within 0.4 nm of at least one of the designated hydrophobic amino acids (Val, Leu, Ile, and Phe), and (iii) each cell was at least 0.8 nm away from the designated hydrophilic amino acids (Lys, Arg, Asp, and Glu). The probe volume near a hydrophilic patch was chosen similarly (Fig. 2a). The probe volumes in confined systems were chosen with the additional constraint that the cells had to be in the region between the two domains (Fig. 2d and 2e).

Melittin: The melittin dimer as well as the tetramer were solvated in ~ 5000 SPC/E water molecules. To study the region between the two dimers, one of the dimers from the tetramer crystal structure (PDB: 2MLT) was translated along the dimer-dimer vector by 0.6, 0.7, 0.8 and 0.9 nm. The backbone atoms of the dimers were constrained harmonically. Bonds within melittin were constrained using the P-LINCS algorithm, while those in the water were constrained with the SETTLE algorithm. Temperature was maintained at 300K using the canonical velocity rescaling thermostat by Bussi and co-workers.

To select the probe volume for a given separation between the dimers, the convex hull of the C^α positions of residues 8 and 20 of each monomer (*i.e.*, 8 points in total) was first calculated, and a 0.1 nm-resolution grid was then placed in the system. Grid cells whose center was (i) inside the convex hull and (ii) outside the van der Waals radius of each protein heavy atom were selected to be part of the probe volume. The probe volume thus constructed was slightly different for each mutant. To select a probe volume near an isolated dimer, the convex hull for separation of 0.4 nm between the wild-type dimers was computed. Grid cells in this convex hull that do not overlap with protein heavy atoms of one of the dimers constitute the probe volume of that dimer. The same probe volume was used for all mutant

dimers, allowing a direct comparison of density fluctuations near them.

Additionally, in all BphC and melittin simulations, electrostatic interactions were calculated using the particle-mesh Ewald algorithm, and the net charge on the protein was neutralized by adding the requisite numbers of Na^+ or Cl^- ions.

Supplementary Figure

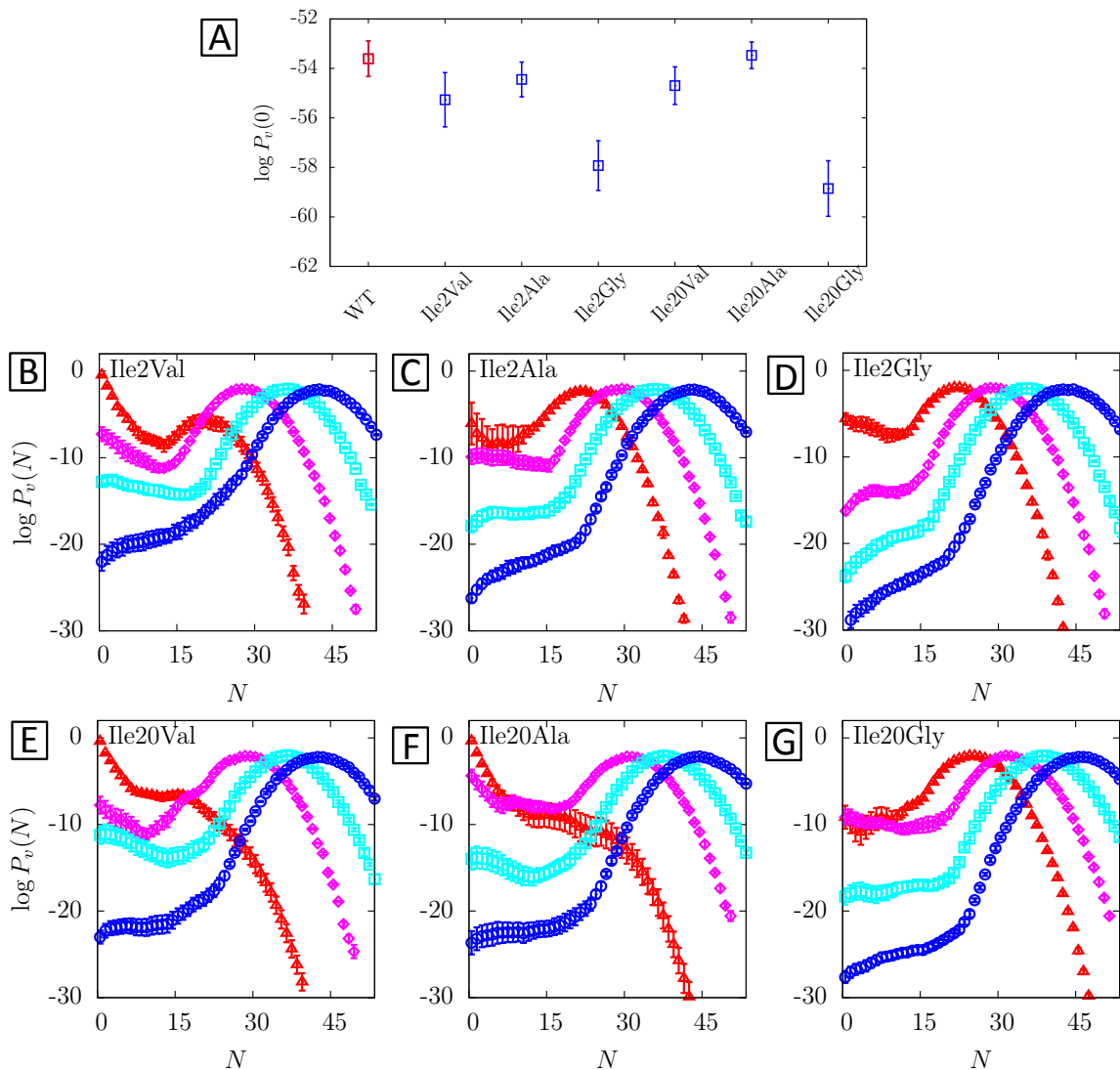


Figure S1. Water density fluctuations for mutant melittin dimers and tetramers. (A) $\log P_v(0)$ for probe volume v near six mutant melittin dimers, compared to that near the wild-type dimer. Mutating the more hydrophobic Ile residue (at position 2 or 20) in the wild-type dimer to Val, Ala, and Gly reduces the value of $\log P_v(0)$. (B), (C), and (D) show $\log P_v(N)$ for probe volume v between mutant melittin dimers, Ile2Val, Ile2Ala, and Ile2Gly, respectively, for dimer-dimer separations, Δz , of 0.9 (blue), 0.8 (cyan), 0.7 (magenta), and 0.6 nm (red). Mutating Ile2 to Ala or Gly destabilizes the dry state to the extent that the space between dimers is wet even at $\Delta z = 0.6$ nm. (E), (F), and (G) show similar data for mutations of Ile20. In this case, only the Ile20Gly mutant is wet at $\Delta z = 0.6$ nm.